Bootstrapping Multi-atlas Hippocampal Segmentation with MAGeT-Brain

Pipitone J., Winterburn J., Lett, T., Lerch J., Pruessner J., Lepage M.,
Voineskos A., Chakravarty M.M., and
the Alzheimer's Disease Neuroimaging Initiative

June 4, 2013

Abstract

Neuroimaging research often relies on automated anatomical segmentations of MR images of the brain. Current multi-atlas based approaches provide accurate segmentations of brain images by propagating manually derived segmentations of specific neuroanatomical structures to unlabelled data. These approaches often rely on a large number of such manually segmented atlases that take significant time and expertise to produce. We present an algorithm for the automatic segmentation of the hippocampus that minimizes the number of atlases needed while still achieving similar accuracy to multi-atlas approaches.

finish

1 Introduction

The hippocampus is a neuroanatomical structure situated in the medial temporal lobe of the brain, and has long been associated with learning and memory (den Heijer et al., 2012; Scoville and Milner, 2000). In addition to its known functional roles, the hippocampus is of interest to neuroscientists because it is implicated in several forms of brain disfunction such as Alzheimer's disease (Sabuncu et al., 2011) and schizophrenia (Narr et al., 2004; Karnik-Henry et al., 2012). In neuroimaging experiments, magnetic resonance images (MRI) are often used for the identification of the hippocampus. As such, accurate segmentation of the hippocampus and its subregions in MRI is a necessary first step to better understand the unique neuroanatomy of subjects. Typically, the gold standard for neuroanatomical segmentation is manual delineation by an expert human. However the rapid increase in the availability of MRI data and the time and expertise required for manual segmentation is prohibitive (Mazziotta et al., 1995, 2001; Mazziotta et al.; Pausova et al., 2007; ?). Further, there is little agreement between researchers regarding how exactly the hippocampus should be identified in MRI images (Geuze et al., 2004) and this has led to efforts to create an unified hippocampal segmentation protocol (Jack et al., 2011).

Automated segmentation techniques that are reliable, objective, and reproducible are a necessary alternative to manual segmentation. In the case of classical model-based segmentation methods (Haller et al., 1997; Csernansky et al., 1998), an MRI atlas that was previously manually labelled by an expert rater is matched to target images using nonlinear registration methods. The resulting nonlinear transformation is applied to the manual labels (ie. *label propagation*) to apply them to the target image. While this methodology has been used successfully in several contexts (??Collins et al., 1995; Haller et al., 1997), it is limited in accuracy by the introduction of errors due inaccuracies in the nonlinear transformation itself, partial volume effects in label resampling, and irreconcilable differences between the neuroanatomy represented within the atlas and target images.

One methodology that can be used to mitigate these sources of errors involves the use of multiple manually segmented atlases and probabilistic segmentation techniques, such as those found in the FreeSurfer package (Fischl et al., 2002), FreeSurfer uses a probabilistic atlas of anatomical and tissue classes along with spatial constraints for class labels encoded using a Markov random field model to segment the entire brain.

More recently, many groups have been using multiple atlases to improve overall segmentation accuracy (ie. multi-atlas segmentation) over model-based approaches (Heckemann et al., 2006, 2011; Collins and Pruessner, 2010; Lötjönen et al., 2010; Aljabar et al., 2009; Leung et al., 2010; Wolz et al., 2010). Each atlas image is registered to a target image, and label propagation is performed to produce several labellings of the target image (one from each atlas). A *label fusion* technique, such as voxel-wise voting, is used to merge these labels into a definitive segmentation for the target. In addition, weighted voting procedures that use *atlas selection* techniques are often used to exclude atlases from label fusion that are dissimilar to a target image in order to reduce error from unrepresentative anatomy (Aljabar et al., 2009). This involves the selection of a subset of atlases using a similarity metric such a cross-correlation (Aljabar et al., 2009) or normalized mutual information. Such selection has the added benefit of significantly reducing the number of nonlinear registrations. For example Collins and Pruessner (Collins and Pruessner, 2010) demonstrated that only 14 atlases, selected based on highest similarity between medial temporal lobe neuroanatomy as evaluated by normalized mutual information (Studholme et al., 1999) from a library of 80 atlases, were required to achieve accurate segmentations of the hippocampus. Several methods have been explored for label fusion including the STAPLE algorithm (Warfield et al., 2004) that computes a probabilistic segmentation using an expectation maximization framework from an set of competing segmentations; or others where a subset of segmentations can be estimated using metrics such as the sum of squared differences in the regions of interest to be segmented (Coupé et al., 2012).

However, many of these methods require significant investment of time and resources for the creation of the atlas library; ranging from atlas libraries that require between 30 (Heckemann et al., 2006) and 80 (Collins and Pruessner, 2010) manually segmented atlases. This strategy has the main drawback of being inflexible as it does not easily accommodate varying the definition of the hippocampal anatomy (such as the commonly used heuristic of subdividing the hippocampus in to head, body, and tail (Poppenk and Moscovitch, 2011; Pruessner et al., 2000)). Furthermore, none of these methods have demonstrated sufficient flexibility to accommodate atlases that are somehow exceptional such as those derived from serial histological data (?Yelnik et al., 2007) or high-resolution MRI data that enables robust identification of hippocampal subfields (Winterburn et al., 2013; Yushkevich et al., 2009; Mueller and Weiner, 2009; Van Leemput et al., 2009; Wisse et al., 2012). Due to the recent availability of the latter, there has been increased interest in the use of probabilistic methods for the identification of the hippocampal subfields on standard T1-weighted images. Our group recently demonstrated that through use of an intermediary automated segmentation stage, robust and accurate segmentation of the striatum, pallidum, and thalamus using a single atlas derived from serial histological data (?) is possible. The novelty of this manuscript is the extension our multi-atlas methodology to the hippocampus using more than a single input atlas, while simultaneously limiting the number of possible inputs used during segmentation, and demonstrating that accurate identification of the hippocampal subfields is indeed possible using this methodology.

There are few methods that have attempted to perform multi-atlas segmentation with a limited number of input atlases. The LEAP algorithm is an elegant modification to the basic multi-atlas strategy (Wolz et al., 2010) in which the atlas library is grown, beginning with a set of manually labelled atlases, and successively incorporating unlabelled target images after themselves being labelling using multi-atlas techniques. The sequence in which target images are labelled is chosen so that the similarity between the atlas images and the target images is minimised at each step, effectively allowing for deformations between very dissimilar images to be broken up into sequences of smaller deformations. Although Wolz et al. begin with an atlas library of 30 MR images, this method could theoretically work using a much smaller atlas library. In their validation, LEAP was used to segment the whole hippocampus in the ADNI1 baseline dataset, achieving a mean Dice score of 0.85 with manual segmentations.

To the best of our knowledge there are two other segmentation methods that attempt to define the hippocampal subfields using standard T1-weighted data. The first is included with the FreeSurfer package (Van Leemput et al., 2009). This work is limited as it omits the tail of the hippocampus and the segmentation protocol has yet to be fully validated. Nonetheless, they demonstrate that the applicability of their work using data from 10 subjects. In the second method, Yushkevich and colleagues (Yushkevich et al., 2009) acquired and labelled hippocampal subfields on high-resolution MRI data from post-mortem medial temporal lobe samples an demonstrate it's applicability in the segmentation of other MRI-volumes using nonlinear registration guided using manually derived hippocampus masks and specific landmarks. In their work they demonstrate accurate parcellations of the subfields.

Here we address the issue of limiting the number of input atlases by tuning our algorithm, for segmentation of the entire hippocampus, using a multi-fold experiment performed on a subset Alzheimer's Disease Neuroimaging Initiative (ADNI) 1 dataset. Based on the parameters we find in our experiment, we validate our algorithm using all of the data available in the ADNI Complete 1Yr sample and compare our segmentations to the other segmentations that are available through the ADNI informatics portal. To ensure that we have not over-fit our parameters to the aging or neurodegenerative brain, we also apply our segmentations to a dataset of normal controls and individuals suffering from first episode psychosis. Finally, we perform a leave-one-out validation experiment to determine if the subfields can be accurately identified using our multi-atlas framework.

2 Methods

2.1 The MAGeT-Brain Algorithm

In this paper, we will use the term *label* to mean any segmentation (manual or derived) of an MR image. *Label propagation*, or *labelling*, is the process by which two images are registered and the resulting transformation is applied to the labels from one image to bring them into alignment with the other image. We will use the term *atlas* to mean a manually segmented image, and the term *template* to mean an automatically segmented image (i.e. via label propagation). The terms *atlas library* and *template library* describe any set of such images.Additionally, we will use the term *target* to refer to an unlabelled image that is undergoing segmentation.

The simplest form of multi-atlas segmentation, (which we will call *basic multi-atlas segmentation*), involves three steps. First, each labelled input image (i.e. atlas or template) is registered to an unlabelled target image. Second, the labels from each image are propogated to the target image space. Third, the labels are combined into a single labelling by way of a label fusion method (Heckemann et al., 2006, 2011). This method is described in detail in other publications (Collins and Pruessner, 2010; Heckemann et al., 2011; Aljabar et al., 2009).

MAGeT-Brain bootstraps the creation of a large template library given a limited input atlas library, and then uses the template library in basic multi-atlas segmentation. Images for the template library are selected from a set of input target images, either arbitrarily or so as to reflect the neuroanatomy or demographics of the target set as a whole (for instance, by sampling equally from cases and controls). The template library images are then labelled by each of the atlases. Basic multi-atlas segmentation is then conducted using the template library to segment the entire set of target images (including the targets whose images are used in the construction of the template library). Since each template library image has multiple labels (one from each atlas), the final number of labels to be fused for each target may be quite large (i.e. # of atlas × # of templates).

Figure 1 describes the MAGeT-Brain algorithm in pseudocode. Source code for MAGeT-Brain can be found at `http://github.com/pipitone/MAGeTbrain`.

Algorithm 1 Pseudocode for the MAGeT-Brain algorithm

```
function BasicMultiAtlasSegmentation(Templates, Subjects)
    for all target do
        for all template do
            propagate all labels for template to target space
            store target labels
        end for
        fuse target labels
    end for
end function

function MAGeTBrain(Subjects, Atlases, n)
    for i = 1 → n do
        choose a target to be used as a template
        propagate labels from each atlas to template space
        store the template with all of its labels
    end for
    MultiAtlas(Templates, Subjects)
end function
```

Table 1: ADNI-1 cross-validation subset demographics

	CN $N = 23$	LMCI $N = 23$	AD $N = 23$	Combined $N = 69$
Age at baseline Years	72.2 75.5 78.5	71.0 77.1 81.4	71.7 77.8 81.8	71.5 76.6 81.3
Sex : Female	43% (10)	43% (10)	43% (10)	43% (30)
Education	16.0 16.0 18.0	15.0 16.0 18.0	12.0 16.0 16.5	14.0 16.0 18.0
Ethnicity : Unknown	0% (0)	0% (0)	0% (0)	0% (0)
Not Hisp/Latino	100% (23)	100% (23)	100% (23)	100% (69)
Hisp/Latino	0% (0)	0% (0)	0% (0)	0% (0)
CDR-SB	0.00 0.00 0.00	0.75 1.50 1.50	4.00 4.50 5.00	0.00 1.50 4.00
ADAS 13	4.67 5.67 12.34	14.34 16.00 20.50	23.83 29.00 31.66	10.00 16.00 25.33
MMSE	28.5 29.0 30.0	25.0 27.0 28.0	21.0 23.0 24.0	24.0 27.0 29.0

$a\ b\ c$ represent the lower quartile a, the median b, and the upper quartile c for continuous variables.
Numbers after percents are frequencies.

2.2   Experiments

The following section describes the experiments we conducted to assess the segmentation quality of the MAGeT-Brain algorithm. The first two experiments assess the validity of MAGeT-Brain using a cross-validation design. Experiment 1 investigates the accuracy of MAGeT-Brain whole hippocampus segmentation over a wide range of parameter settings. This enables us to choose the parameter settings offering the best performance for use in subsequent experiments. Experiment 2 tests hippocampal subfield segmentation quality. The last two experiments assess the validity of the MAGeT-Brain algorithm when applied to different diseases: Alzheimer's disease (Experiment 3) and first episode schizophrenia patients (Experiment 4).

2.2.1   Experiment 1: Whole Hippocampus Cross-Validation

Monte Carlo Cross-Validation (MCCV) (Shao, 1993) was performed using a pool of images and manual hippocampal segmentations from ADNI1 dataset. This form of cross-validation allows us to rigorously validate a large number of parameter settings of MAGeT-Brain (atlas and template library sizes, registration algorithm, and label fusion method) and select the best parameters to use in subsequent experiments.

ADNI1 dataset   69 1.5T images were arbitrarily selected from the baseline scans in the *ADNI1:Complete 1Yr 1.5T* standardized dataset. 23 subjects were chosen from each disease category: cognitively normal (CN), mild cognitive impairment (MCI) and Alzheimer's disease (AD). Demographics for this subset are shown in Table 1. Manual segmentations of the left and right whole hippocampi are available. These labels have been generated using the SNT tool from Medtronic Surgical Navigation Technologies, Louisville, CO (see Supplementary Materials for detailed discussion of the manual segmentation process used).

Clinical, demographic and pre-processed T1-weighted MRI were downloaded by the authors from the ADNI database (adni.loni.ucla.edu) between March 2012 and August 2012. The image dataset download was the "ADNI1:Complete 1Yr 1.5T " standardized dataset available from ADNI [1] (Wyman et al., 2012). This image collection contains uniformly preprocessed images which have been designated to be the "best" after quality control. All images were acquired using 1.5T scanners (General Electric Healthcare, Philips Medical Systems or Siemens Medical Solutions) at multiple sites using the protocol described in (Jack et al., 2008). Representative 1.5T imaging parameters were TR = 2400ms, TI = 1000ms, TE = 3.5ms, flip angle = 8∘, field of view = 240 x 240mm, a $192 \times 192 \times 166$ matrix (x, y, and z directions) yielding a voxel resolution of $1.25 \times 1.25 \times 1.2 mm^3$.

Experiment details   Monte Carlo Cross-Validation (MCCV), also known as repeated random sub-sampling cross-validation, consists of repeated rounds of validation conducted on a fixed dataset Shao (1993). In each round, the dataset is randomly partitioned into a training set and a validation set. The method to be validated is then given the training data, and its output is compared with the validation set.

---

[1]http://adni.loni.ucla.edu/methods/mri-analysis/adni-standardized-data/

Table 2: ANIMAL registration parameters

Parameters	Stage 1	Stage 2	Stage 3
Model Blur (FWHM)	8	8	4
Input Blur (FWHM)	8	8	4
Iterations	30	30	10
Step	8x8x8	4x4x4	2x2x2
Sub-Lattice	6	6	6
Lattice Diameter	24x24x24	12x12x12	6x6x6

In this experiment, our dataset consists of 69 1.5T images and corresponding manual segmentations. In each validation round, the dataset is partitioned into a training set consisting of images and their manual labels to be used as an atlas library, and a validation set consisting of the remaining images segmented by both MAGeT-Brain and multi-atlas. The resulting segmentations are compared to the manual segmentations for the images.

A total of ten validation rounds are perfomed on each subject in the dataset, over each combination of parameter settings. The parameter settings we explore are: atlas library size (1-9), template library size (1-20), registration method (ANTS or ANIMAL), and label fusion method (majority vote, cross-correlation weighted majority vote, and normalized mutual information weighted majority vote). A total of $10 \times 69 \times 9 \times 20 \times 2 \times 3 = 7\,452\,000$ validation rounds were conducted, resulting in a total of $1\,490\,400$ segmentations analysed.

Before registration, all images underwent preprocessing with the N3 algorithm (Sled et al., 1998) to minimize intensity nonuniformity. In this experiment we use one of two non-linear image registration methods.

Automatic Normalization and Image Matching and Anatomical Labeling (ANIMAL) The ANIMAL algorithm carries out image registration is in two phases. In the first, a 12-parameter linear transformation (3 translations, rotations, scales, shears) is estimated between images using an algorithm that maximizes the correlation between blurred MR intensities and gradient magnitude over the whole brain (Collins et al.). In the second phase, nonlinear registration is completed using the ANIMAL algorithm (Collins et al., 1995): an iterative procedure that estimates a 3D deformation field between two MR images. At first, large deformations are estimated using blurred version of the input data. These larger deformations are then input to subsequent steps where the fit is refined by estimating smaller deformations on data blurred with a Gaussian kernel with a smaller FWHM. The final transformation is a set of local translations defined on a bed of equally spaced nodes that were estimated through the optimization of the correlation coefficient. For the purposes of this work we used the regularization parameters optimized in Robbins et al. (Robbins et al., 2004), displayed in table 2.2.1.

Automatic Normalization Tools (ANTS) ANTS is a diffeomorphic registration algorithm which provides great flexibility over the choice of transformation model, objective function, and the consistency of the final transformation. The transformation is estimated in a hierarchical fashion where the MRI data is subsampled, allowing large deformations to be estimated and successively refined at later hierarchical stages (where the data is subsampled to a finer grid). The deformation field and the objective function are regularized with a Gaussian kernel at each level of the hierarchy. The ANTS algorithm is freely available http://www.picsl.upenn.edu/ANTS/. We used an implementation of the ANTS algorithm compatible with the MINC data format, mincANTS https://github.com/vfonov/mincANTS.

We used the following command line when running ANTS :

```
mincANTS 3 -m PR[target_file.mnc,source_file.mnc,1,4]
  --number-of-affine-iterations 10000x10000x10000x10000x10000
  --affine-gradient-descent-option 0.5x0.95x1.e-4x1.e-4
  --use-Histogram-Matching --MI-option 32x16000
  -r Gauss[3,0] -t SyN[0.5] -i 100x100x100x20
  -o transformation.xfm
```

These settings were adapted from the "reasonable starting point" given in the ANTS manual [2].

Label fusion methods   Label fusion is a term given to the process of combining the information from several candidate labellings for an intensity image into a single labelling. In this experiment we explore three fusion methods.

Voxel-wise Majority Vote Labels are propagated from all template library images to a target. Each output voxel is given the most frequent label at that voxel location amongst all candidate labellings. Ties are broken arbitrarily.

Cross-correlation Weighted Majority Vote An optimal combination of targets from the template library has previously been shown to improve segmentation accuracy (Aljabar et al., 2009; Collins and Pruessner, 2010). In this method, each template library image is ranked in similarity to each unlabelled image by the normalized cross-correlation (CC) of image intensities after linear registration, over a region of interest (ROI) generously encompassing the hippocampus. Only the top ranked template library image labels are used in a voxel-wise majority vote. The ROI is heuristically defined as the extent of all atlas labels after linear registration to the template, dilated by three voxels (**?**). The number of top ranked template library image labels is a configurable parameter and displayed as the size of the template library in the rest of the paper.

The `xcorr_vol` utility from the ANIMAL toolkit is used to calculate the cross-correlation similarity measure.

Normalised Mutual Information Weighted Majority Vote This method is similar to cross-correlation weighted voting except that image similarity is calculated by the normalised mutual information score over the region of interest(Studholme et al., 2001). The `itk_similarity` utility from the EZMinc toolkit[3] is used to calculate the normalised mutual information measure between to images.

Evaluation method   The Dice similarity coefficient (DSC) assesses the agreement between two segmentations. It is one of the most widely used measures of segmentation performance, and we use it as the basis of comparison in this experiment. Additionally, we report the Jaccard index, another commonly used similarity measure:

$$\text{Dice's coefficient (DSC)} = \frac{2|A \cap B|}{|A| + |B|}$$

$$\text{Jaccard (J)} = \frac{|A \cap B|}{|A \cup B|} = \frac{DSC}{(2 - DSC)}$$

where A and B are the regions being compared, and the cardinality is the volume measured in voxels.

The manual segmentations (SNT) provided as part of the ADNI dataset are used as the gold standard to compare with. The segmentation accuracy reported is averaged over the ten validation rounds for each parameter setting.

In order to investigate the performance of MAGeT-Brain in a real world setting in which only one set of atlas and template images are used, we explore the variability in label agreement at fixed parameter settings when the choice for atlas and template images is varied. This is achieved by first computing the standard deviation and variance of DSC scores in each block of ten validation rounds per subject. The distribution of these statistics across all subjects is then compared between MAGeT-Brain and multi-atlas using a Student's t-test. A significant difference between distributions is taken to show either a larger or smaller level of variability between methods.

2.2.2   Experiment 2: Winterburn Atlases Cross-Validation

In this experiment, the accuracy of the MAGeT-Brain algorithm on hippocampal subregion segmentation is tested using a leave-one-out cross-validation (LOOCV) design. The optimal parameter settings found in Experiment 1 are used.

---

[2]https://sourceforge.net/projects/advants/files/Documentation/
[3]https://github.com/vfonov/EZminc

Winterburn Atlases dataset   The Winterburn atlases (Winterburn et al., 2013) are digital hippocampal segmentations of five in-vivo 300μ isotropic T1-weighted MR images. The segmentations include subfield segmentations for the cornus ammonis (CA) 1, CA4, dentate gyrus, subiculum, and CA 2 and 3 combined. Subjects in the Winterburn atlases range in age from 29-57 years (mean age of 37), and include two males and three females.

In addition to the high-resolution scans distributed as part of the Winterburn atlases, we also obtained additional 3T T1 BRAVO images (0.9mm-isotropic voxels) of four of the five Winterburn atlas subjects.

Experiment details   Leave-one-out cross-validation (LOOCV) is an approach in which the method to be validated is given all but one item in a dataset as training data, and the output is compared with the left-out item. This is done, in turn, for each item in the dataset.

In this experiment, the five 300μ-isotropic voxel Winterburn atlases are used as the atlas library for MAGeT-Brain segmentation. LOOCV is conducted separately for two different input datasets: the four Winterburn atlas subject T1 BRAVO images (referred to as the *BRAVO* dataset), and the five Winterburn atlas subject images subsampled to 0.9mm-isotropic voxel resolution (referred to as the *Subsampled* dataset. Each subject in the dataset is segmented by MAGeT-Brain with that subject's image excluded from the atlas library. The template library consists of 3T T1 images (0.9mm-isotropic voxels) of healthy subjects in addition to the images from the dataset being evaluated.

The optimal size of template library, registration method, and label fusion method found in Experiment 1 are used.

Evaluation method   MAGeT-Brain performance is measured with respect to straight-forward nearest-neighbour resampling of the Winterburn atlas labels to 0.9mm-isotropic voxels (i.e. no label propagation). The volumes of each hippocampal subregion in the subsampled Winterburn atlas labels are compared to the volumes obtained from the full resolution Winterburn atlas labels, the MAGeT-Brain labels on the subsampled Winterburn atlas images, and the MAGeT-Brain labels on the T1 BRAVO acquisitions.

2.2.3   Experiment 3: Application to the segmentation first episode schizophrenia patients

To validate that MAGeT-Brain algorithm works effectively in the context of other neuropsychiatric disorders, we use the Winterburn atlases with MAGeT-Brain to predict the hippocampal segmentation of dataset of Schizophrenia patient MR images. The resulting segmentations are assessed for quality by comparison with expert manual segmentations.

SZ-FEP dataset   All patients were recruited and treated through the Prevention and Early Intervention Program for Psychoses (PEPP-Montreal), a specialized early intervention service at the Douglas Mental Health University Institute in Montreal, Canada. People aged 1530 years from the local catchment area suffering from either affective or non-affective psychosis who had not taken antipsychotic medication for more than one month with an IQ above 70 were consecutively admitted as either in- or out-patients. Of those treated at PEPP, only patients aged 18 to 30 years with no previous history of neurological disease or head trauma causing loss of consciousness were eligible for the neuroimaging study; only those suffering from schizophrenia spectrum disorders were considered for this analysis. For complete program details see Malla et al. (Malla et al., 2003).

Scanning of 81 subjects was carried out at the Montreal Neurological Institute on a 1.5-T Siemens whole body MRI system. Structural T1 volumes were acquired for each participant using a three-dimensional (3D) gradient echo pulse sequence with sagittal volume excitation (repetition time=22ms, echo time=9.2ms, flip angle=30∘, 180 1mm contiguous sagittal slices). The rectangular field-of-view for the images was 256mm (SI)×204mm (AP). Subject demographics are shown in table 3.

The hippocampus were traced following a validated protocol developed by Dr Jens Pruessner . A recent update to this protocol by Dr J Pruessner in 2006 allows to accurately and consistently subdivide the hippocampus into three different subregions: head, body, and tail. We use these segmentations as to validate our implementation of MAGeT-Brain .

cite: (Pruessner 2000)

Table 3: Schizophrenia First Episode Patient Demographics

	N	FEP
		$N = 81$
Age	80	21 23 26
Gender : M	81	63% (51)
Handedness : ambi	81	6% (5)
left		5% (4)
right		89% (72)
Education	81	11 13 15
SES : lower	81	31% (25)
middle		54% (44)
upper		15% (12)
FSIQ	79	88 102 109

a b c represent the lower quartile a, the median b, and the upper quartile c for continuous variables.
N is the number of non–missing values.
Numbers after percents are frequencies.

Experiment details MAGeT-Brain is configured with an atlas library composed of the Winterburn T1 atlases (see Experiment 2). All images from the SZ-FEP dataset are segmented. The optimal size of template library, registration method, and label fusion method found in Experiment 1 are used.

Evaluation method The manual segmentation protocol used to segment the Winterburn atlases has some neuroanatomical differences in comparison to the protocol used to segment the SZFEP dataset. Therefore, rather than evaluate using an overlap metric, such as DSC, which assumes a fixed segmentation protocol, we instead correlate whole hippocampus volume between MAGeT-Brain and manual segmentations.

done elsewhe

2.2.4   Experiment 4: Application to the segmentation of Alzheimer's disease patients

To validate that MAGeT-Brain algorithm works as well as established automated methods, MAGeT-Brain is applied to the ADNI1 dataset and the resulting segmentations are compared to those produced by FreeSurfer, FSL, MAPER, and by expert manual segmentation.

ADNI1 dataset revisited All images from the *ADNI1:Complete 1Yr 1.5T* standardized dataset described in Experiment 1 are used. Clinical and demographic data are shown in table **??**.

Experiment details MAGeT-Brain is configured with an atlas library composed of the Winterburn T1 atlases (see Experiment 2). All images from the ADNI1:Complete 1Yr 1.5T dataset are segmented. The optimal size of template library, registration method, and label fusion method found in Experiment 1 are used. The template library is composed of equal numbers of images from each disease class (AD, MCI, and cognitively normal controls).

Evaluation method Since the hippocampal segmentation protocols differ between the ADNI labels and Winterburn atlases, this poses a problem for direct evaluation between labels produced by MAGeT-Brain and the ADNI labels in terms of overlap; we would not expect different segmentation protocols to have a high degree of overlap. Instead, to evaluate the performance of MAGeT-Brain we compare the correlation of MAGeT-Brain segmentation volumes with manual segmentation (SNT) volumes. Additionally, we correlate the hippocampal volumes of established automated segmentation methods to MAGeT-Brain segmentations.

Table 4: ADNI1 1.5T Complete 1Yr dataset demographics

	N	CN $N = 584$	LMCI $N = 931$	AD $N = 404$	Combined $N = 1919$
Age at baseline Years	1919	72.4 75.8 78.5	70.5 75.1 80.4	70.1 75.3 80.2	71.1 75.3 79.8
Sex : Female	1919	48% (278)	35% (327)	49% (198)	42% (803)
Education	1919	14 16 18	14 16 18	12 15 17	13 16 18
Ethnicity : Unknown	1919	2% (9)	1% (6)	1% (3)	1% (18)
Not Hisp/Latino		97% (569)	97% (904)	99% (401)	98% (1874)
Hisp/Latino		1% (6)	2% (21)	0% (0)	1% (27)
CDR-SB	1911	0.0 0.0 0.0	1.0 1.5 2.5	3.5 4.5 6.0	0.0 1.5 3.0
ADAS 13	1895	5.67 8.67 12.33	14.67 19.33 24.33	24.67 30.00 35.33	10.67 18.00 25.33
MMSE	1917	29 29 30	25 27 29	20 23 25	25 27 29

a b c represent the lower quartile a, the median b, and the upper quartile c for continuous variables.
N is the number of non–missing values.
Numbers after percents are frequencies.

3 Results

3.1 Experiment 1 Results: Whole Hippocampus Cross-Validation

In this experiment we conducted 10 rounds of MAGeT-Brain and multi-atlas segmentation of each of 69 subjects at a range of atlas and template library sizes, registration algorithm (ANTS or ANIMAL), and three label fusion techniques. Hippocampal MAGeT-Brain -based segmentations using both ANIMAL and ANTS registration algorithm demonstrate good overlap with SNT derived gold-standards (Figure **??**). Qualitatively, both ANIMAL and ANTS -based segmentations demonstrate trend overlap accuracy that increases with the size of atlas library and template library. Improvement in accuracy diminishes noticeably with template libraries larger than roughly ten images.

No marked difference in segmentation accuracy is seen when either ANIMAL or ANTS registration is used with any number of atlases or templates. In every parameter configuration, the use of MAGeT-Brain with ANTS registration shows a pronounced increase in segmentation accuracy over MAGeT-Brain with ANIMAL registration. Surprisingly, the label fusion method used does not significantly improve label accuracy, contrary to the findings of Aljabar et al. Aljabar et al. (2009) when using weighted voting on much larger altas/template libraries. In the remainder of this section, only results using the ANTS registration algorithm and majority vote fusion will be shown.

With an increasing number of templates, MAGeT-Brain shows improvement in overlap accuracy over multi-atlas-based segmentation when using the same number of atlases and voting method (Figure **??**). The magnitude of improvement over multi-atlas-based segmentation decreases with an increasing number of atlases, with accuracy converging with 7 atlases. Peak improvement in MAGeT-Brain accuracy (0.02 DSC) is found when one atlas is used with a template library of 20 images.

In addition to an improvement in accuracy over multi-atlas-based segmentation, MAGeT-Brain also shows a decrease in the variability of segmentation accuracy (Figure 3). The size of template library necessary to reach a significant (p¡0.5) decrease in variance and standard deviation grows with the size of atlas library used. A template library of 19 images is sufficient to show significant decrease in variance and standard deviation for 3-7 atlases.

It is interesting to note that with an even number of templates, MAGeT-Brain shows a small decrease in performance relative to when one fewer template image is used. See section for a discussion of this behaviour. In the remainder of this section, only results from odd-sized template libraries will be shown.
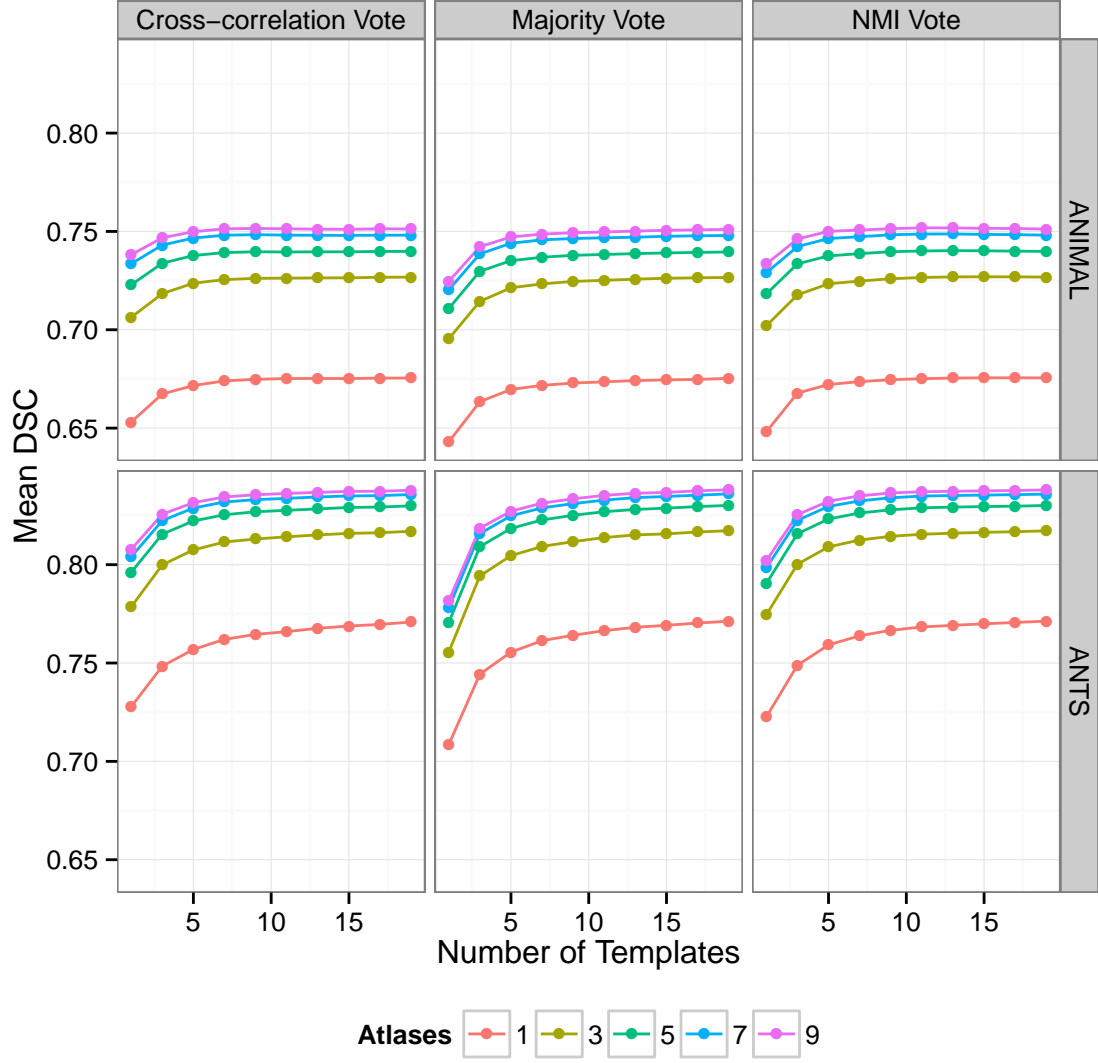
9

Figure 1: **Mean DSC of MAGeT-Brain segmentations across 69 ADNI1 subjects, by atlas and template library size, registration algorithm, and label fusion method.**
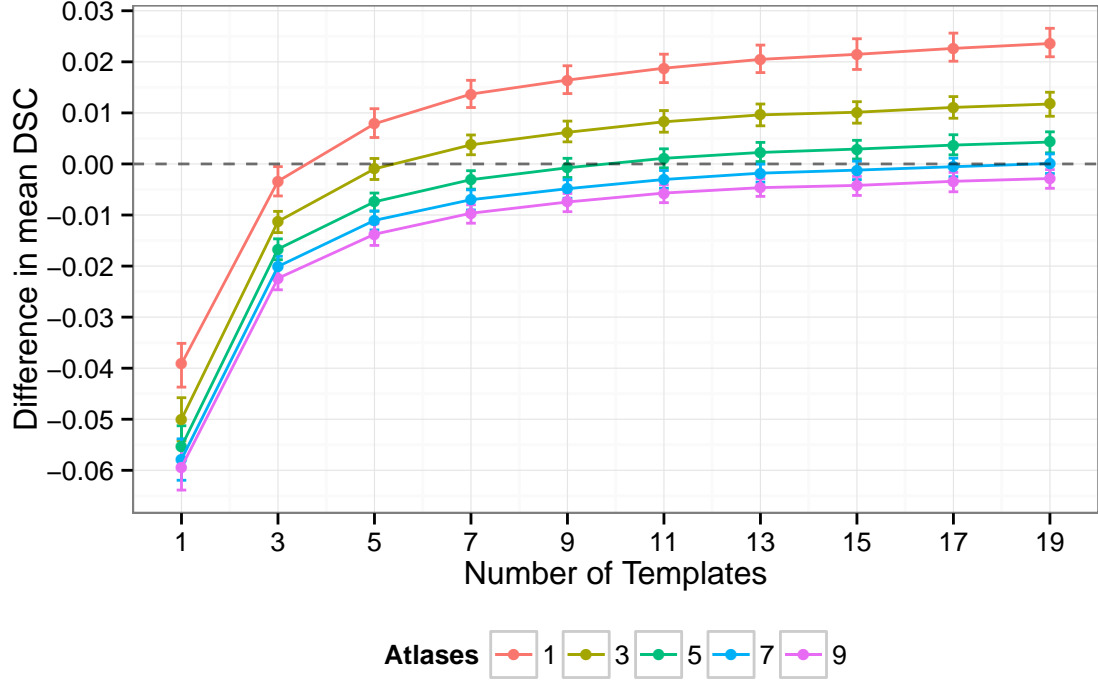
Figure 2: The difference in mean DSC between MAGeT-Brain and multi-atlas segmentations for a range of parameter settings.

Error: arguments imply differing number of rows: 79, 0

Figure 3: **Difference in variability of MAGeT-Brain vs. multi-atlas segmentation accuracy.** Variance of segmentation accuracy between MAGeT-Brain and multi-atlas segmentation is computed for each subject across all ten rounds of validation. Shown on the y-axis (scaled logarithmically) is the p-value resulting from a t-test comparing the distribution of variances at each parameter setting (atlas/template library size). Only points where MAGeT-Brain mean variability is lower than multi-atlas are shown.

3.2 Experiment 2 Results: Winterburn Atlases Cross-Validation

This experiment explores MAGeT-Brain segmentations of hippocampal subfields. To achieve this, a leave-one-out validation is conducted in which lower-resolution images ($0.9mm^3$ voxels) of each Winterburn atlas subject is segmented using the remaining Winterburn atlases. As a point of comparison, volumes of Winterburn atlases when subsampled to $0.9mm^3$ voxels are also computed.

In general, across hippocampal subregions the percent error in volume between MAGeT-Brain segmentations and the manual Winterburn atlas segmentations compares favourably to error when resampling the atlas segmentations (Figure 4). In particular, the CA1, CA4, and Dentate subregions all show near or smaller percent errors. The Sibiculum and CA2/CA3 subregions show distinctly larger volumes than resampling error. .

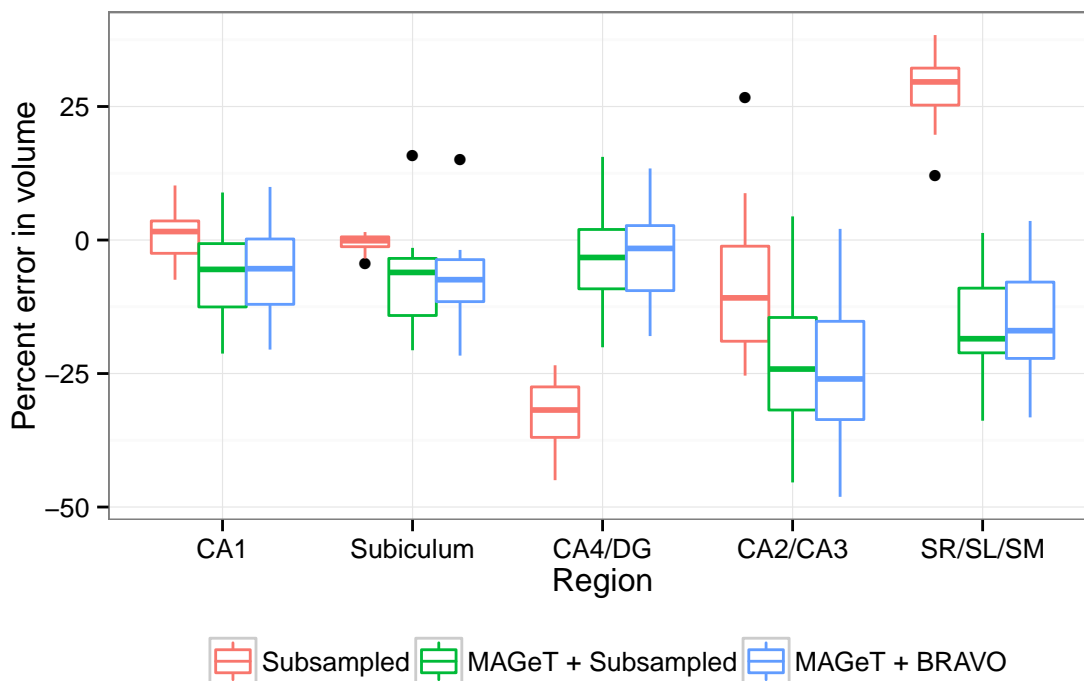Figure 5 shows a qualitative comparision of MAGeT-Brain subfield segmentation.

Figure 4: **Percent error in segmentation volume by hippocampus subregion.** Percent error is measured against the volumes of of the unmodified Winterburn atlas segmentations. **Subsampled** are volumes of the manual segmentations of the Winterburn atlases after resampling to $0.9mm^3$. **MAGeT + WA Subsampled** volumes are MAGeT-Brain segmentations of the Winterburn atlas images after resampling to $0.9mm^3$ voxels. **MAGeT + WA BRAVO** volumes are MAGeT-Brain segmentations of T1 BRAVO images ($0.9mm^3$ voxels) acquired separately of four of the five Winterburn atlas subjects.
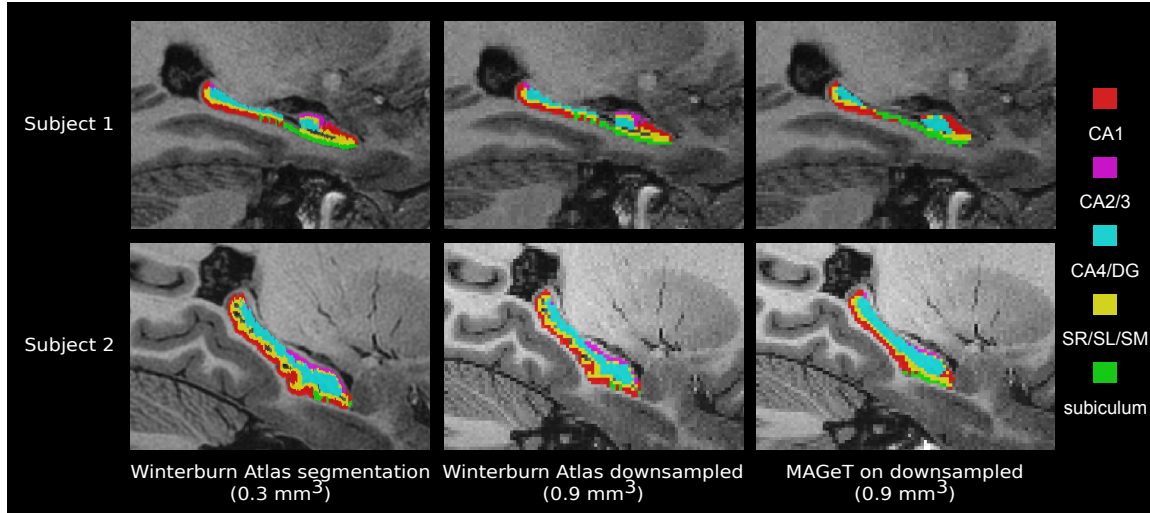
Figure 5: Sagittal slices from two subjects showing a comparison of the original Winterburn atlas subfield segmentations (at 0.3mm3-isotropic voxel resolution), the subsampled Winterburn segmentations (at 0.9mm3-isotropic voxel resolution), and the MAGeT brain labels on the subsampled atlas image.

3.3 Experiment 3 Results: Application to the segmentation of first episode schizophrenia patients

In this experiment MAGeT-Brain is applied to a dataset of images of first episode schizophrenia parients, using the Winterburn atlases and a template library of 21 subject images selected at random. Expert manual whole hippocampal segmentations are used as gold standards.

MAGeT-Brain produces hippocampus segmentation volumes that are highly correlated with manual segmentation volumes (Figure 6). p-value
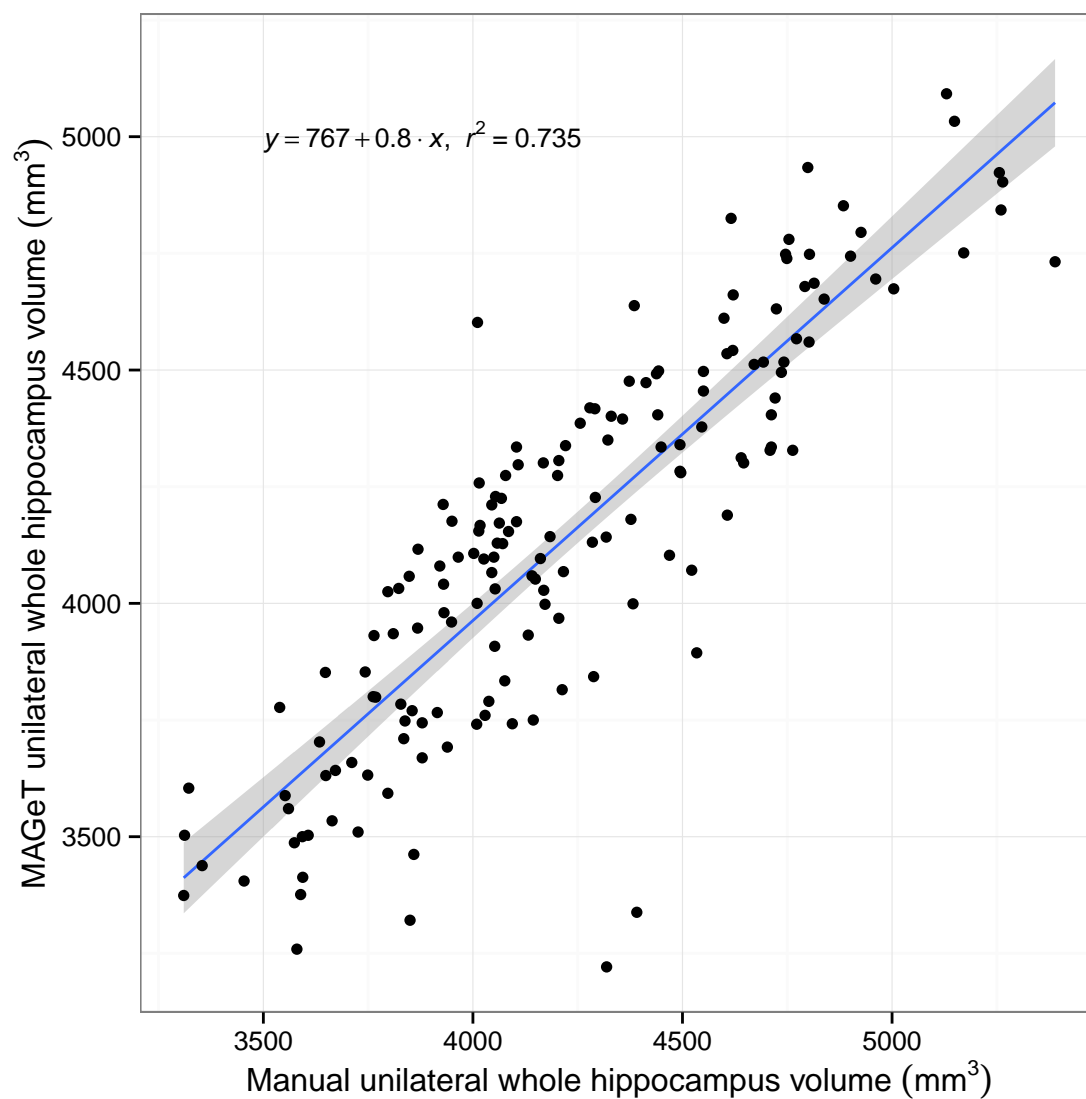
Figure 6: **First Episode Schizophrenic Patients.** Comparison of total HC volumes for MAGeT-Brain against manually rated Hippocampal volumes

Table 5: Pass/fail quality control indicators were supplied with the FreeSurfer volumes downloaded from the ADNI website (we used the temporal lobe quality control indicator, TEMPQC). One of the authors (MP) performed visual quality inspection for MAGeT and FSL segmentations.

	X	Total	SNT	MAGeT	MAPER	FSL	FS
1	Images	1909	1445	1909	636	1876	1530
2	Failures	N/A	–	34	–	27	304

3.4 Experiment 4 Results: Application to the segmentation of Alzheimer's disease patients

Based on the results from the ADNI1 Cross-Validation experiment, in this experiment MAGeT-Brain was configured with a template library of 21 randomly chosen subject images (7 from each disease class) and used majority vote label fusion. The entire ADNI1:Complete 1Yr 1.5T dataset was segmented by MAGeT-Brain and we now compare the resulting volumes with those obtained by manual segmentation (SNT), and other automated segmentation techniques (MAPER, FreeSurfer, and FSL). Table ?? shows the total count of segmentations available, including a count of those which have failed a quality control inspection. Only those images which had segmentations from every method are included in the following analysis (a total of 361 images; Table 5).

We find a close relationship in total bilateral hippocampal volume between all methods and manually segmented volumes (Figure 8). Volumes are correlated with Pearson-r ¿ 0.78 for all methods across disease categories. Within disease categories (Figure 7), MAGeT-Brain is consistently well correlated to manual volumes (Pearson-r ¿ 0.85), but appears to slightly over-estimate the volume of the AD hippocampus.

To investigate the level of agreement with manually segmented hippocampal volumes, we constructed Bland-Altman plots for each method (Figure ??). As Bland & Altman, 1985 ? noted, high correlation amongst measures of the same quantity does not necessarily imply agreement (as correlation can be driven by a large range in true values, for instance). What is most striking in Figure ?? is that all methods show an obvious proportional bias: FreeSurfer and FSL markedly under-estimate smaller hippocampi and over-estimate large hippocampi, whereas MAPER and MAGeT-Brain more conservatively show the reverse bias. Additionally, all methods show a fixed bias, with FreeSurfer and FSL most dramatically over-estimating hippocampal volume by $2600mm^3$ and $2800mm^3$ on average, respectively, and MAPER and MAGeT-Brain within $250mm^3$ on average.

Figure 10 shows a qualitative comparison of MAGeT-Brain and manual (SNT) hippocampal segmentations for 10 randomly selected subjects in each disease category, and illustrates some of the common errors found during visual inspection. Mostly frequently, we find MAGeT-Brain improperly includes the vestigial hippocampal sulcus and, although not anatomically incorrect, MAGeT-Brain under-estimates the hippocampal body in comparison to the manual (SNT) segmentation.
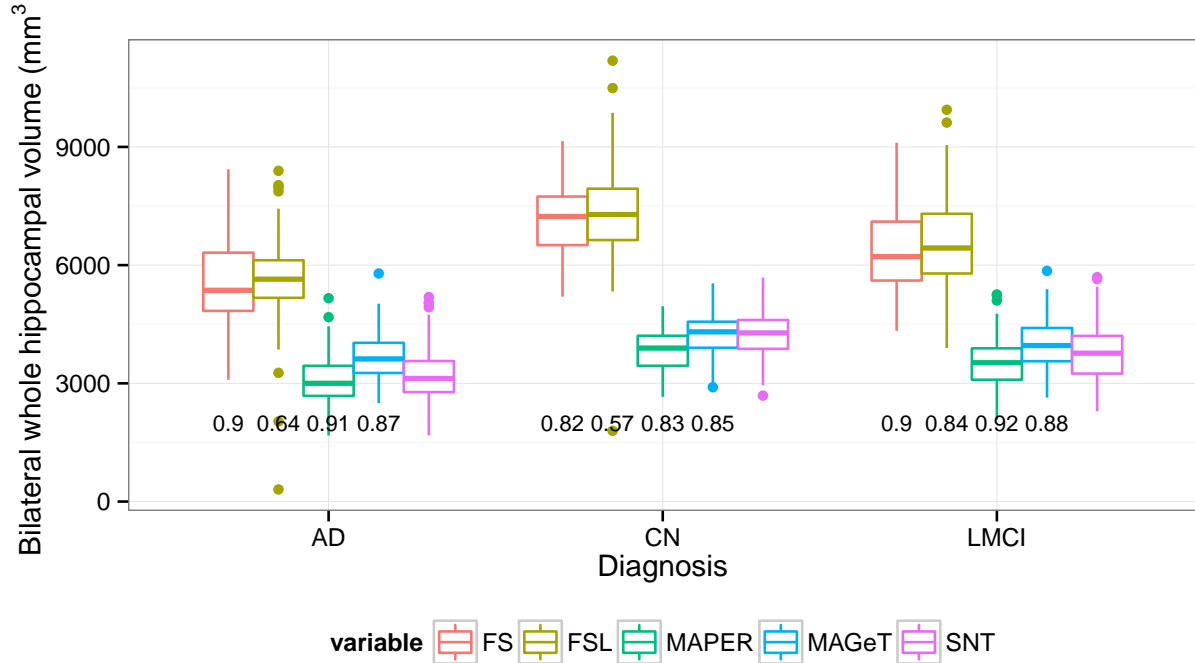
Figure 7: Comparison of hippocampus volumes obtained by FreeSurfer (FS), FSL, MAPER, MAGeT-Brain (MAGeT) and manual (SNT) by disease category. Pearson correlation with manual volumes are shown below each box-and-whisker.
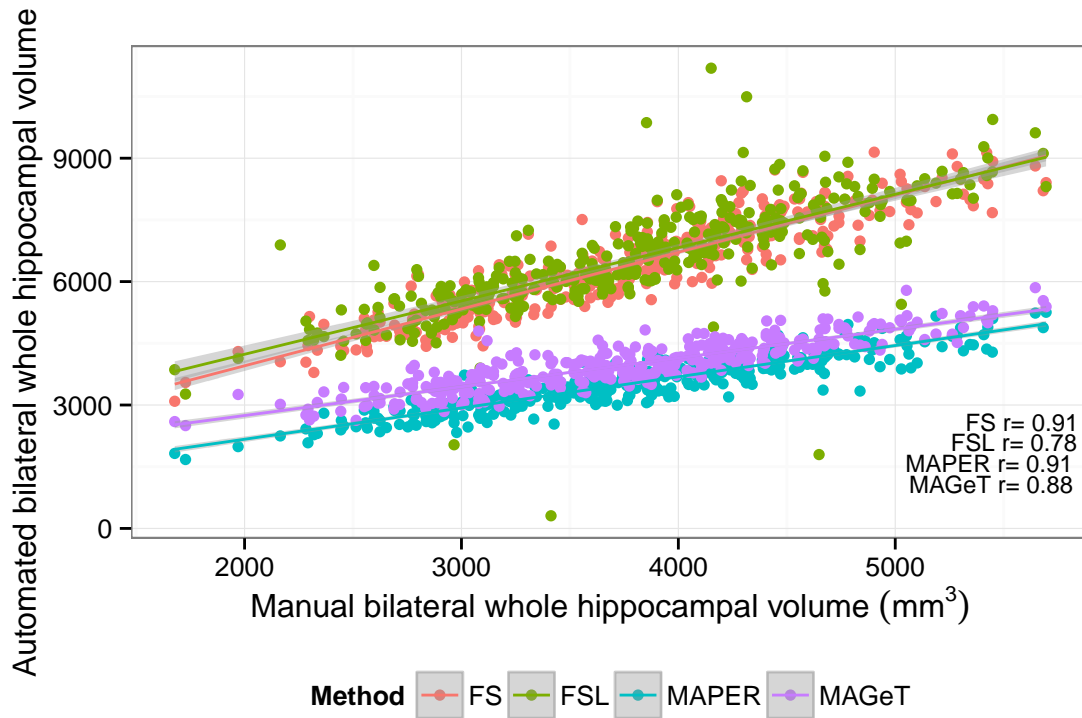

Figure 8: Comparison of hippocampus volumes obtained by FreeSurfer (FS), FSL, MAPER, MAGeT-Brain (MAGeT) and manual (SNT). Pearson correlation with manual volumes are shown for each method.
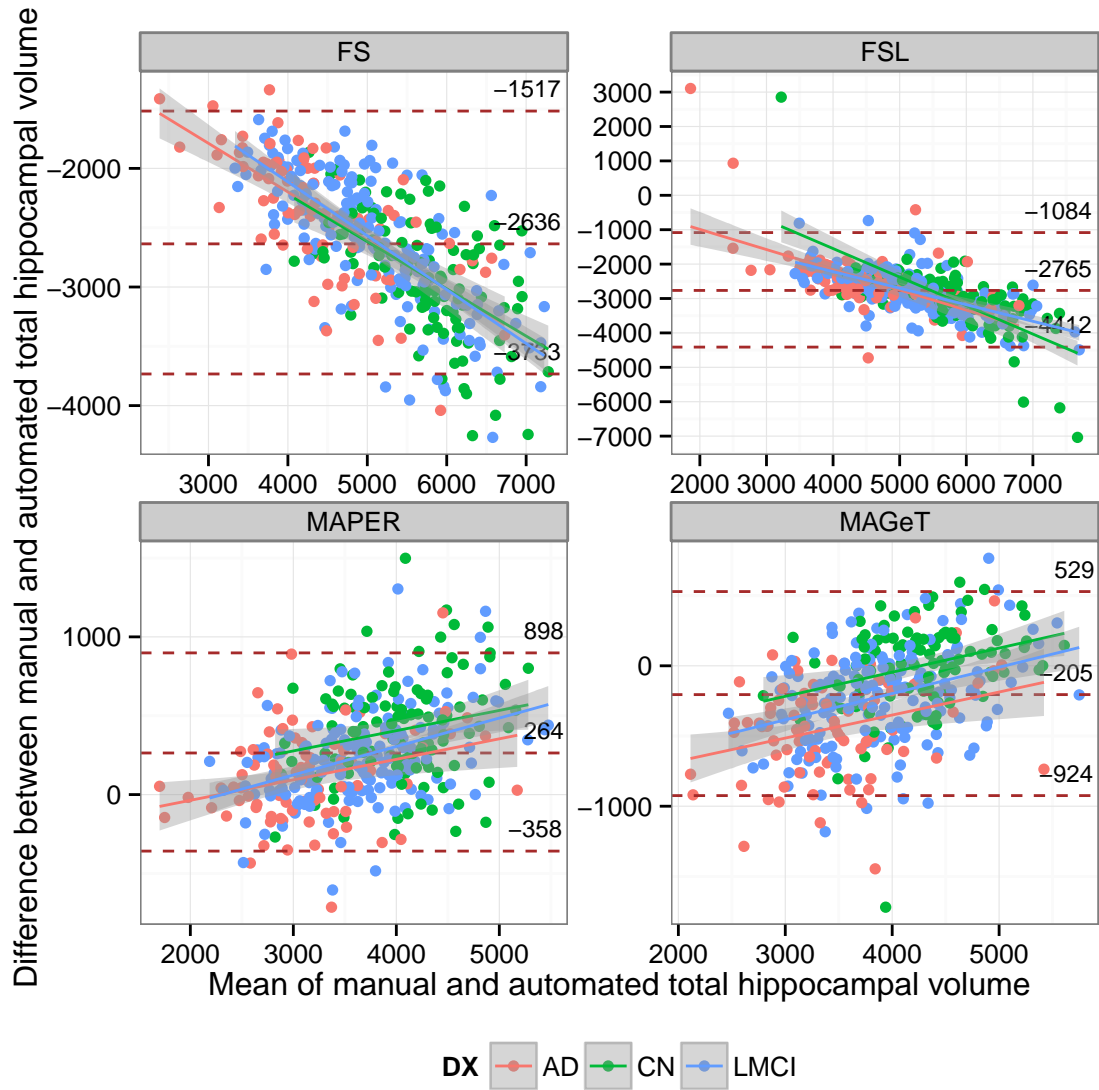
Figure 9: Bland-Altman plot comparing manual (SNT) and automated total hippocampal volumes in the ADNI1:Complete 1Yr 1.5T dataset. The overall mean difference, and limits of agreement ($\pm 1.96 SD$) are shown by dashed horizontal lines.
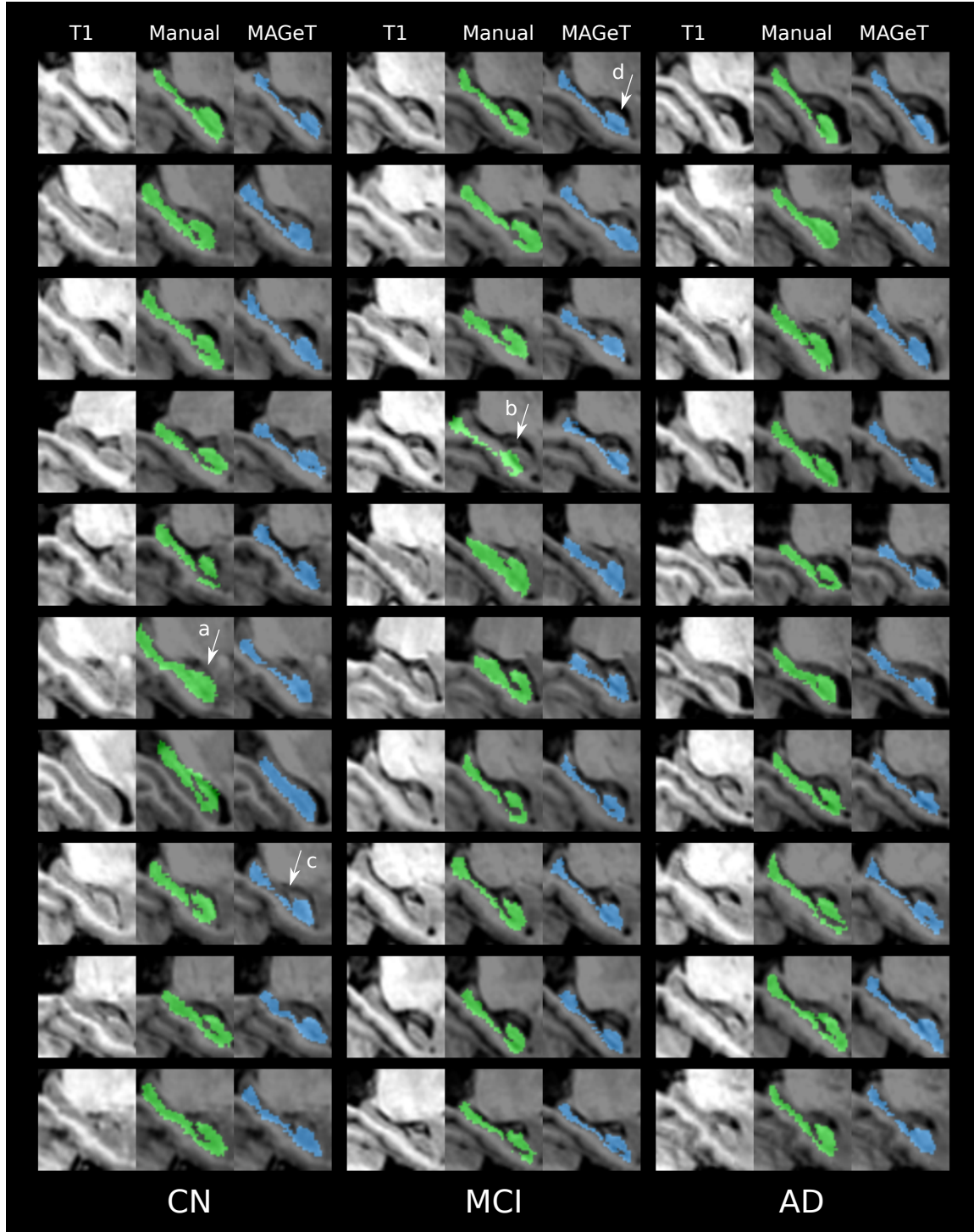
Figure 10: Manual and MAGeT segmentation results for 30 ADNI1 subjects (10 subjects randomly selected from each disease category in the subject pool used in Experiment 1). Sagittal slices are shown for subject unlabelled T1-weighted anatomical image, SNT manual label (green), and MAGeT-Brain label (blue). Noted are examples of common segmentation idiosyncracies: *(a)* over-estimation of hippocampal head and *(b)* translated manual segmentation by SNT; *(c)* under-estimation of hippocampal body and *(d)* improper inclusion of the vestigial hippocampal sulcus by MAGeT-Brain .

Table 6: Survey of automated segmentation accuracy of the ADNI dataset

Method	Atlases	DSC	Reference
Multi-atlas	30	0.775	Wolz et al. (2010)
LEAP (N=300)	30	0.808	Wolz et al. (2010)
Multi-atlas 2	30	0.82	Wolz et al. (2010)
LEAP (N=1)	30	0.838	Wolz et al. (2010)
		0.84 (AD)	Coupé et al. (2012)
LEAP (N=300)	30	0.848	Wolz et al. (2010)
prob. atlas in MNI space	16	0.86 (AD)	Chupin et al. (2009)
AdaBoost +	20	0.86	Morra et al. (2008)
prob. atlas in MNI space	16	0.87 (CN)	Chupin et al. (2009)
		0.88 (CN)	Coupé et al. (2012)
Multi-atlas	13	0.885	Lötjönen et al. (2010)
Multi-atlas (MAPS)	55	0.9	Leung et al. (2010)

4   Discussion

```
Experiment 1:
- address the absence of weighted-voting effects.
  - hypothesis: the benefits of weighted voting only outweigh the resampling
    error effects when choosing from a large library.  In this experiment, the
    template library (during weighted voting) consists of only 20 templates, so
    the most we could hope for is a "squashing" upwards of the curve towards
    the 20-template limit (which is the same across all cases in this experiment).
  - we do see a slight "squashing" effect, with XCORR more strongly than NMI.
    Perhaps in future experiments with larger template libraries, this could be
    explored further.
- Why don't we use STAPLE? What would we expect from STAPLE or other fusion methods?
  - couldn't get STAPLE to work with our image formats
  - Idea: expect smoothness across range of templates (no even # dips, below)
  - perhaps more sophisticated fusion methods would boost results over majority
    vote based techniques.

- why does MAGeT brain show a dip in average Kappa when using an even number
  templates. Does MA show this same pattern? (yes)
  - Hypothesis: our voting method is biased when breaking ties to choose the
    label with the lowest numeric value.
  - If we compute the total number of labels fused (atlases * templates) then
    both MB/MA perform worse when fusing an even number of labels.

- we only show a +0.02 increase in mean Kappa over multi-atlas, and this is when
  using 1 atlas (which we know from Figure 2, is when we perform worst). Why does
  this increase justify the extra effort involved in MB?
  - decrease in variability
  - we are comparing "true" averages (see above)... does this make our criteria
    for a worthy improvement less strict?


- how does MAGeT stack up, Kappa-wise, to other methods, in an absolute sense.
- because of the extensive cross-validation in experiment 1, we are very likely
  showing results that approach the true average of MB and MA on that dataset
  (i.e. our mid 0.8 range result is a mean across 69 subjects and 10 repetitions
  each).
- even with this caveat, do we think we do well enough?  i.e. other than parameter
```

tuning, to what extent does this experiment tell us about how MB would do in
practice.

- effects we are seeing is not only averaging effects (Chakravarty et al. 2012).

- take aways: as in other studies (Aljabar, Heckemann) we find that performance
  scales with the number of inputs (approx. log(n)), and that a large enough
  template library can boost performance with a small number of atlases. The use
  of templates /can/ have a negative impact on performance (Figure 2), that is
  balanced by the improvement of growing the template library. Likely the negative
  impact on peformance is as a result of resampling/mislabelling error. In other
  words, tuning MAGeT brain involves balancing the tension between an improvement
  in peformance due to increase neuroanatomical capture and decreased peformance
  due to resampling error.

Experiment 2:
- describe resampling error during downsampling (essentially partial volume effect
  due to averaging/majority vote in nearest neighbour selection)
- Why would some structures have greater downsampling error than others? (i.e. what
  is it about a structure that would make it especially prone to resampling error)
  - since error is discretised to whole voxels, smaller regions will show larger
    percent error
  - average unilateral volume (approx; mm3):
     region   volume   downsampling error
     CA1   800   2%
     CA4/DG   600   -30%
     SR/SL/SM 700   30%
     Sibculum 350   0%
     CA2/3   200   15%

- observation: when downsampling error is small (<10 percent), MB error is larger,
  and vice versa when downsampling error is large. Could this a case where the
  inevitable MAGeT resampling error outweighs the small downsampling error?
- observation: MAGeT produces similar volumes for the downsampled and BRAVO images
  which demonstrates reliability. Additionally, MB's error is in the same *direction*
  as the downsampling error except for SR/SL/SM
- for MB to show less error than resampling means that voting across templates is
  in aggregate performing better than local nearest neighbour fitting. presumably
  we'd see the same improvement with basic multiatlas as well.

- take away: MB produces subregion volumes that are comparable or better than
  resampling error, except for the CA2/3 where error is near 25 percent (but
  even then resampling error is ~15%)

Experiment 3:
- what is an "acceptable" r^2 value?
- take away: MB has proven to be robust with atlases derived from three different
  segmentation protocols (SNT, Winterburn, and now Pruessner) on three different
  populations (older with AD progression; young and healthy; young and SZ).

Experiment 4:
- address the smaller difference in mean volume across disease classes. smaller
  than every other method.

- address the segmentation bias towards over-estimating smaller hippocampi, and
  underestimating larger HC

- visual inspection/QC reveals MB segmentations are satisfactory (failure rate
  is lower than the other methods (but we may be biased. :-).

- take away: MB, with the Winterburn atlases, produces HC volumes more inline with
  SNT than FSL/FS. Comparable to MAPER but with far fewer atlases required.

5 Conclusion

6 Supplementary Materials

6.1 ADNI Manual Labels

Semi-automated hippocampal volumetry was carried out using a commercially available high dimensional brain mapping tool (Medtronic Surgical Navigation Technologies, Louisville, CO), that has previously been validated and compared to manual tracing of the hippocampus (Hsu et al., 2002). Measurement of hippocampal volume is achieved first by placing manually 22 control points as local landmarks for the hippocampus on the individual brain MRI data: one landmark at the hippocampal head, one at the tail, and four per image (i.e., at the superior, inferior, medial and lateral boundaries) on five equally spaced images perpendicular to the long axis of the hippocampus. Second, fluid image transformation is used to match the individual brains to a template brain (Christensen et al., 1997). The pixels corresponding to the hippocampus are then labeled and counted to obtain volumes. This method of hippocampal voluming has a documented reliability of an intraclass coefficient better than .94 (Hsu et al., 2002).

References

P Aljabar, R a Heckemann, a Hammers, J V Hajnal, and D Rueckert. Multi-atlas based segmentation of brain images: atlas selection and its effect on accuracy. *NeuroImage*, 46(3):726–38, July 2009. ISSN 1095-9572. doi: 10.1016/j.neuroimage.2009.02.018. URL http://www.ncbi.nlm.nih.gov/pubmed/19245840.

G E Christensen, S C Joshi, and M I Miller. Volumetric transformation of brain anatomy. *IEEE transactions on medical imaging*, 16(6):864–77, December 1997. ISSN 0278-0062. doi: 10.1109/42.650882. URL http://ieeexplore.ieee.org/xpl/articleDetails.jsp?arnumber=650882.

Marie Chupin, Emilie Gérardin, Rémi Cuingnet, Claire Boutet, Louis Lemieux, Stéphane Lehéricy, Habib Benali, Line Garnero, and Olivier Colliot. Fully automatic hippocampus segmentation and classification in Alzheimer's disease and mild cognitive impairment applied on data from ADNI. *Hippocampus*, 19(6): 579–87, June 2009. ISSN 1098-1063. doi: 10.1002/hipo.20626. URL http://www.pubmedcentral.nih.gov/articlerender.fcgi?artid=2837195\&tool=pmcentrez\&rendertype=abstract.

D L Collins, P Neelin, T M Peters, and A C Evans. Automatic 3D intersubject registration of MR volumetric data in standardized Talairach space. *Journal of computer assisted tomography*, 18(2):192–205. ISSN 0363-8715. URL http://www.ncbi.nlm.nih.gov/pubmed/8126267.

D Louis Collins and Jens C Pruessner. Towards accurate, automatic segmentation of the hippocampus and amygdala from MRI by augmenting ANIMAL with a template library and label fusion. *NeuroImage*, 52 (4):1355–66, October 2010. ISSN 1095-9572. doi: 10.1016/j.neuroimage.2010.04.193. URL http://www.ncbi.nlm.nih.gov/pubmed/20441794.

D. Louis Collins, C. J. Holmes, T. M. Peters, and A. C. Evans. Automatic 3-D model-based neuroanatomical segmentation. *Human Brain Mapping*, 3(3):190–208, October 1995. ISSN 10659471. doi: 10.1002/hbm. 460030304. URL http://doi.wiley.com/10.1002/hbm.460030304.

Pierrick Coupé, Simon F Eskildsen, José V Manjón, Vladimir S Fonov, and D Louis Collins. Simultaneous segmentation and grading of anatomical structures for patient's classification: application to Alzheimer's disease. *NeuroImage*, 59(4):3736–47, February 2012. ISSN 1095-9572. doi: 10.1016/j.neuroimage.2011.10.080. URL `http://www.ncbi.nlm.nih.gov/pubmed/22094645`.

John G Csernansky, Sarang Joshi, Lei Wang, John W Haller, Mokhtar Gado, J Philip Miller, Ulf Grenander, and Michael I Miller. Hippocampal morphometry in schizophrenia by high dimensional brain mapping. *Proceedings of the National Academy of Sciences of the United States of America*, 95(19):11406–11411, 1998. URL `http://www.pubmedcentral.nih.gov/articlerender.fcgi?artid=21655\&tool=pmcentrez\&rendertype=abstract`.

T den Heijer, F Van der Lijn, M W Vernooij, M de Groot, P J Koudstaal, a Van der Lugt, G P Krestin, a Hofman, W J Niessen, and M M B Breteler. Structural and diffusion MRI measures of the hippocampus and memory performance. *NeuroImage*, 63(4):1782–9, December 2012. ISSN 1095-9572. doi: 10.1016/j.neuroimage.2012.08.067. URL `http://www.ncbi.nlm.nih.gov/pubmed/22960084`.

Bruce Fischl, David H Salat, Evelina Busa, Marilyn Albert, Megan Dieterich, Christian Haselgrove, Andre van der Kouwe, Ron Killiany, David Kennedy, Shuna Klaveness, Albert Montillo, Nikos Makris, Bruce Rosen, and Anders M Dale. Whole brain segmentation: automated labeling of neuroanatomical structures in the human brain. *Neuron*, 33(3):341–55, January 2002. ISSN 0896-6273. URL `http://www.ncbi.nlm.nih.gov/pubmed/11832223`.

E. Geuze, E. Vermetten, and J D Bremner. MR-based in vivo hippocampal volumetrics: 2. Findings in neuropsychiatric disorders. *Molecular Psychiatry*, 10(2):160, September 2004. doi: 10.1038/sj.mp.4001579. URL `http://www.nature.com.myaccess.library.utoronto.ca/mp/journal/v10/n2/full/4001579a.htmlhttp://www.nature.com.myaccess.library.utoronto.ca/mp/journal/v10/n2/pdf/4001579a.pdf`.

J W Haller, A Banerjee, G E Christensen, M Gado, S Joshi, M I Miller, Y Sheline, M W Vannier, and J G Csernansky. Three-dimensional hippocampal MR morphometry with high-dimensional transformation of a neuroanatomic atlas. *Radiology*, 202(2):504–510, 1997. URL `http://www.ncbi.nlm.nih.gov/entrez/query.fcgi?cmd=Retrieve\&db=PubMed\&dopt=Citation\&list\_uids=9015081`.

Rolf A. Heckemann, Joseph V. Hajnal, Paul Aljabar, Daniel Rueckert, and Alexander Hammers. Automatic anatomical brain MRI segmentation combining label propagation and decision fusion. *NeuroImage*, 46(3):726–38, July 2006. ISSN 1095-9572. doi: 10.1016/j.neuroimage.2009.02.018. URL `http://www.ncbi.nlm.nih.gov/pubmed/19245840`.

Rolf A Heckemann, Shiva Keihaninejad, Paul Aljabar, Katherine R Gray, Casper Nielsen, Daniel Rueckert, Joseph V Hajnal, and Alexander Hammers. Automatic morphometry in Alzheimer's disease and mild cognitive impairment. *NeuroImage*, 56(4):2024–37, July 2011. ISSN 1095-9572. doi: 10.1016/j.neuroimage.2011.03.014. URL `http://www.pubmedcentral.nih.gov/articlerender.fcgi?artid=3153069\&tool=pmcentrez\&rendertype=abstract`.

Yuan-Yu Hsu, Norbert Schuff, An-Tao Du, Kevin Mark, Xiaoping Zhu, Dawn Hardin, and Michael W Weiner. Comparison of automated and manual MRI volumetry of hippocampus in normal aging and dementia. *Journal of magnetic resonance imaging : JMRI*, 16(3):305–10, September 2002. ISSN 1053-1807. doi: 10.1002/jmri.10163. URL `http://www.pubmedcentral.nih.gov/articlerender.fcgi?artid=1851676\&tool=pmcentrez\&rendertype=abstract`.

Clifford R Jack, Matt A Bernstein, Nick C Fox, Paul Thompson, Gene Alexander, Danielle Harvey, Bret Borowski, Paula J Britson, Jennifer L Whitwell, Chadwick Ward, Anders M Dale, Joel P Felmlee, Jeffrey L Gunter, Derek L G Hill, Ron Killiany, Norbert Schuff, Sabrina Fox-Bosetti, Chen Lin, Colin Studholme, Charles S DeCarli, Gunnar Krueger, Heidi A Ward, Gregory J Metzger, Katherine T Scott, Richard Mallozzi, Daniel Blezek, Joshua Levy, Josef P Debbins, Adam S Fleisher, Marilyn Albert, Robert Green, George Bartzokis, Gary Glover, John Mugler, and Michael W Weiner. The Alzheimer's Disease Neuroimaging Initiative (ADNI): MRI methods. *Journal of magnetic resonance imaging : JMRI*, 27(4):

685–91, April 2008. ISSN 1053-1807. doi: 10.1002/jmri.21049. URL `http://www.pubmedcentral.nih.gov/articlerender.fcgi?artid=2544629\&tool=pmcentrez\&rendertype=abstract`.

Clifford R Jack, Frederik Barkhof, Matt A Bernstein, Marc Cantillon, Patricia E Cole, Charles Decarli, Bruno Dubois, Simon Duchesne, Nick C Fox, Giovanni B Frisoni, Harald Hampel, Derek L G Hill, Keith Johnson, Jean-François Mangin, Philip Scheltens, Adam J Schwarz, Reisa Sperling, Joyce Suhy, Paul M Thompson, Michael Weiner, and Norman L Foster. Steps to standardization and validation of hippocampal volumetry as a biomarker in clinical trials and diagnostic criterion for Alzheimer's disease. *Alzheimer's & dementia : the journal of the Alzheimer's Association*, 7(4):474–485.e4, July 2011. ISSN 1552-5279. doi: 10.1016/j.jalz.2011.04.007. URL `http://www.ncbi.nlm.nih.gov/pubmed/21784356`.

Meghana S Karnik-Henry, Lei Wang, Deanna M Barch, Michael P Harms, Carolina Campanella, and John G Csernansky. Medial temporal lobe structure and cognition in individuals with schizophrenia and in their non-psychotic siblings. *Schizophrenia research*, 138(2-3):128–35, July 2012. ISSN 1573-2509. doi: 10.1016/j.schres.2012.03.015. URL `http://www.ncbi.nlm.nih.gov/pubmed/22542243`.

Kelvin K Leung, Josephine Barnes, Gerard R Ridgway, Jonathan W Bartlett, Matthew J Clarkson, Kate Macdonald, Norbert Schuff, Nick C Fox, and Sebastien Ourselin. Automated cross-sectional and longitudinal hippocampal volume measurement in mild cognitive impairment and Alzheimer's disease. *NeuroImage*, 51(4):1345–59, July 2010. ISSN 1095-9572. doi: 10.1016/j.neuroimage.2010.03.018. URL `http://www.pubmedcentral.nih.gov/articlerender.fcgi?artid=2873209\&tool=pmcentrez\&rendertype=abstract`.

Jyrki Mp Lötjönen, Robin Wolz, Juha R Koikkalainen, Lennart Thurfjell, Gunhild Waldemar, Hilkka Soininen, and Daniel Rueckert. Fast and robust multi-atlas segmentation of brain magnetic resonance images. *NeuroImage*, 49(3):2352–65, March 2010. ISSN 1095-9572. doi: 10.1016/j.neuroimage.2009.10.026. URL `http://dx.doi.org/10.1016/j.neuroimage.2009.10.026`.

Ashok Malla, Ross Norman, Terry McLean, Derek Scholten, and Laurel Townsend. A Canadian programme for early intervention in non-affective psychotic disorders. *The Australian and New Zealand journal of psychiatry*, 37(4):407–13, August 2003. ISSN 0004-8674. URL `http://www.ncbi.nlm.nih.gov/pubmed/12873324`.

J Mazziotta, A Toga, A Evans, P Fox, J Lancaster, K Zilles, R Woods, T Paus, G Simpson, B Pike, C Holmes, L Collins, P Thompson, D MacDonald, M Iacoboni, T Schormann, K Amunts, N Palomero-Gallagher, S Geyer, L Parsons, K Narr, N Kabani, G Le Goualher, J Feidler, K Smith, D Boomsma, H Hulshoff Pol, T Cannon, R Kawashima, and B Mazoyer. A four-dimensional probabilistic atlas of the human brain. *Journal of the American Medical Informatics Association : JAMIA*, 8(5):401–30. ISSN 1067-5027. URL `http://www.pubmedcentral.nih.gov/articlerender.fcgi?artid=131040\&tool=pmcentrez\&rendertype=abstract`.

J Mazziotta, A Toga, A Evans, P Fox, J Lancaster, K Zilles, R Woods, T Paus, G Simpson, B Pike, C Holmes, L Collins, P Thompson, D MacDonald, M Iacoboni, T Schormann, K Amunts, N Palomero-Gallagher, S Geyer, L Parsons, K Narr, N Kabani, G Le Goualher, D Boomsma, T Cannon, R Kawashima, and B Mazoyer. A probabilistic atlas and reference system for the human brain: International Consortium for Brain Mapping (ICBM). *Philosophical transactions of the Royal Society of London. Series B, Biological sciences*, 356(1412):1293–322, August 2001. ISSN 0962-8436. doi: 10.1098/rstb.2001.0915. URL `http://www.pubmedcentral.nih.gov/articlerender.fcgi?artid=1088516\&tool=pmcentrez\&rendertype=abstract`.

J C Mazziotta, A W Toga, A Evans, P Fox, and J Lancaster. A probabilistic atlas of the human brain: theory and rationale for its development. The International Consortium for Brain Mapping (ICBM). *NeuroImage*, 2(2):89–101, June 1995. ISSN 1053-8119. URL `http://www.ncbi.nlm.nih.gov/pubmed/9343592`.

Jonathan H Morra, Zhuowen Tu, Liana G Apostolova, Amity E Green, Christina Avedissian, Sarah K Madsen, Neelroop Parikshak, Xue Hua, Arthur W Toga, Clifford R Jack, Michael W Weiner, and Paul M Thompson. Validation of a fully automated 3D hippocampal segmentation method using subjects with

Alzheimer's disease mild cognitive impairment, and elderly controls. *NeuroImage*, 43(1):59–68, October 2008. ISSN 1095-9572. doi: 10.1016/j.neuroimage.2008.07.003. URL `http://www.pubmedcentral.nih.gov/articlerender.fcgi?artid=2624575\&tool=pmcentrez\&rendertype=abstract`.

Susanne G Mueller and Michael W Weiner. Selective effect of age, Apo e4, and Alzheimer's disease on hippocampal subfields. *Hippocampus*, 19(6):558–64, June 2009. ISSN 1098-1063. doi: 10.1002/hipo.20614. URL `http://www.pubmedcentral.nih.gov/articlerender.fcgi?artid=2802542\&tool=pmcentrez\&rendertype=abstract`.

Katherine L Narr, Paul M Thompson, Philip Szeszko, Delbert Robinson, Seonah Jang, Roger P Woods, Sharon Kim, Kiralee M Hayashi, Dina Asunction, Arthur W Toga, and Robert M Bilder. Regional specificity of hippocampal volume reductions in first-episode schizophrenia. *NeuroImage*, 21(4):1563–75, April 2004. ISSN 1053-8119. doi: 10.1016/j.neuroimage.2003.11.011. URL `http://www.ncbi.nlm.nih.gov/pubmed/15050580`.

Zdenka Pausova, Tomás Paus, Michal Abrahamowicz, Jason Almerigi, Nadine Arbour, Manon Bernard, Daniel Gaudet, Petr Hanzalek, Pavel Hamet, Alan C Evans, Michael Kramer, Luc Laberge, Susan M Leal, Gabriel Leonard, Jackie Lerner, Richard M Lerner, Jean Mathieu, Michel Perron, Bruce Pike, Alain Pitiot, Louis Richer, Jean R Séguin, Catriona Syme, Roberto Toro, Richard E Tremblay, Suzanne Veillette, and Kate Watkins. Genes, maternal smoking, and the offspring brain and body during adolescence: design of the Saguenay Youth Study. *Human brain mapping*, 28(6):502–18, June 2007. ISSN 1065-9471. doi: 10.1002/hbm.20402. URL `http://www.ncbi.nlm.nih.gov/pubmed/17469173`.

Jordan Poppenk and Morris Moscovitch. A Hippocampal Marker of Recollection Memory Ability among Healthy Young Adults: Contributions of Posterior and Anterior Segments. *Neuron*, 72 (6):931–937, December 2011. ISSN 0896-6273. doi: 10.1016/j.neuron.2011.10.014. URL `http://www.sciencedirect.com/science/article/pii/S089662731100924Xhttp://pdn.sciencedirect.com.myaccess.library.utoronto.ca/science?_ob=MiamiImageURL\&_cid=272195\&_user=994540\&_pii=S089662731100924X\&_check=y\&_origin=article\&_zone=toolbar\&_coverDate=22-Dec-2011\&view=c\&originContentFamily=serial\&wchp=dGLbVlV-zSkzk\&md5=e75d94a1de9d5c31e146f910b38468da/1-s2.0-S089662731100924X-main.pdfhttp://www.sciencedirect.com.myaccess.library.utoronto.ca/science/article/pii/S089662731100924X`.

J C Pruessner, L M Li, W Serles, M Pruessner, D L Collins, N Kabani, S Lupien, and A C Evans. Volumetry of hippocampus and amygdala with high-resolution MRI and three-dimensional analysis software: minimizing the discrepancies between laboratories. *Cerebral cortex (New York, N.Y. : 1991)*, 10(4):433–42, April 2000. ISSN 1047-3211. URL `http://www.ncbi.nlm.nih.gov/pubmed/10769253`.

Steven Robbins, Alan C Evans, D Louis Collins, and Sue Whitesides. Tuning and comparing spatial normalization methods. *Medical image analysis*, 8(3):311–23, September 2004. ISSN 1361-8415. doi: 10.1016/j.media.2004.06.009. URL `http://www.ncbi.nlm.nih.gov/pubmed/15450225`.

Mert R Sabuncu, Rahul S Desikan, Jorge Sepulcre, Boon Thye T Yeo, Hesheng Liu, Nicholas J Schmansky, Martin Reuter, Michael W Weiner, Randy L Buckner, Reisa a Sperling, and Bruce Fischl. The dynamics of cortical and hippocampal atrophy in Alzheimer disease. *Archives of neurology*, 68(8):1040–8, August 2011. ISSN 1538-3687. doi: 10.1001/archneurol.2011.167. URL `http://www.pubmedcentral.nih.gov/articlerender.fcgi?artid=3248949\&tool=pmcentrez\&rendertype=abstract`.

W B Scoville and B Milner. Loss of recent memory after bilateral hippocampal lesions. 1957. *The Journal of neuropsychiatry and clinical neurosciences*, 12(1):103–113, 2000. URL `http://www.ncbi.nlm.nih.gov/pubmed/10678523`.

Jun Shao. Linear Model Selection by Cross-validation. *Journal of the American Statistical Association*, 88 (422):486–494, June 1993. ISSN 0162-1459. doi: 10.1080/01621459.1993.10476299. URL `http://www.tandfonline.com/doi/abs/10.1080/01621459.1993.10476299`.

J G Sled, a P Zijdenbos, and a C Evans. A nonparametric method for automatic correction of intensity nonuniformity in MRI data. *IEEE transactions on medical imaging*, 17(1):87–97, February 1998. ISSN 0278-0062. doi: 10.1109/42.668698. URL `http://www.ncbi.nlm.nih.gov/pubmed/9617910`.

C. Studholme, D.L.G. Hill, and D.J. Hawkes. An overlap invariant entropy measure of 3D medical image alignment. *Pattern Recognition*, 32(1):71–86, January 1999. ISSN 00313203. doi: 10.1016/S0031-3203(98)00091-0. URL http://dx.doi.org/10.1016/S0031-3203(98)00091-0.

C Studholme, E Novotny, I G Zubal, and J S Duncan. Estimating tissue deformation between functional images induced by intracranial electrode implantation using anatomical MRI. *NeuroImage*, 13(4):561–76, April 2001. ISSN 1053-8119. doi: 10.1006/nimg.2000.0692. URL http://www.ncbi.nlm.nih.gov/pubmed/11305886.

Koen Van Leemput, Akram Bakkour, Thomas Benner, Graham Wiggins, Lawrence L Wald, Jean Augustinack, Bradford C Dickerson, Polina Golland, and Bruce Fischl. Automated segmentation of hippocampal subfields from ultra-high resolution in vivo MRI. *Hippocampus*, 19(6):549–57, June 2009. ISSN 1098-1063. doi: 10.1002/hipo.20615. URL http://www.pubmedcentral.nih.gov/articlerender.fcgi?artid=2739884\&tool=pmcentrez\&rendertype=abstract.

Simon K Warfield, Kelly H Zou, and William M Wells. Simultaneous truth and performance level estimation (STAPLE): an algorithm for the validation of image segmentation. *IEEE transactions on medical imaging*, 23(7):903–21, July 2004. ISSN 0278-0062. doi: 10.1109/TMI.2004.828354. URL http://www.pubmedcentral.nih.gov/articlerender.fcgi?artid=1283110\&tool=pmcentrez\&rendertype=abstract.

Julie L Winterburn, Jens C Pruessner, Sofia Chavez, Mark Schira, Nancy J Lobaugh, Aristotle N Voineskos, and M Mallar Chakravarty. A novel in vivo atlas of human hippocampal subfields using high-resolution 3T magnetic resonance imaging. *NeuroImage*, 74:254–65, February 2013. ISSN 1095-9572. doi: 10.1016/j.neuroimage.2013.02.003. URL http://www.ncbi.nlm.nih.gov/pubmed/23415948.

L E M Wisse, L Gerritsen, J J M Zwanenburg, H J Kuijf, P R Luijten, G J Biessels, and M I Geerlings. Subfields of the hippocampal formation at 7 T MRI: in vivo volumetric assessment. *NeuroImage*, 61(4):1043–9, July 2012. ISSN 1095-9572. doi: 10.1016/j.neuroimage.2012.03.023. URL http://www.ncbi.nlm.nih.gov/pubmed/22440643.

Robin Wolz, Paul Aljabar, Joseph V Hajnal, Alexander Hammers, and Daniel Rueckert. LEAP: learning embeddings for atlas propagation. *NeuroImage*, 49(2):1316–25, January 2010. ISSN 1095-9572. doi: 10.1016/j.neuroimage.2009.09.069. URL http://www.pubmedcentral.nih.gov/articlerender.fcgi?artid=3068618\&tool=pmcentrez\&rendertype=abstract.

Bradley T Wyman, Danielle J Harvey, Karen Crawford, Matt A Bernstein, Owen Carmichael, Patricia E Cole, Paul K Crane, Charles Decarli, Nick C Fox, Jeffrey L Gunter, Derek Hill, Ronald J Killiany, Chahin Pachai, Adam J Schwarz, Norbert Schuff, Matthew L Senjem, Joyce Suhy, Paul M Thompson, Michael Weiner, and Clifford R Jack. Standardization of analysis sets for reporting results from ADNI MRI data. *Alzheimer's & dementia : the journal of the Alzheimer's Association*, October 2012. ISSN 1552-5279. doi: 10.1016/j.jalz.2012.06.004. URL http://www.ncbi.nlm.nih.gov/pubmed/23110865.

Jérôme Yelnik, Eric Bardinet, Didier Dormont, Grégoire Malandain, Sébastien Ourselin, Dominique Tandé, Carine Karachi, Nicholas Ayache, Philippe Cornu, and Yves Agid. A three-dimensional, histological and deformable atlas of the human basal ganglia. I. Atlas construction based on immunohistochemical and MRI data. *NeuroImage*, 34(2):618–38, January 2007. ISSN 1053-8119. doi: 10.1016/j.neuroimage.2006.09.026. URL http://www.ncbi.nlm.nih.gov/pubmed/17110133.

Paul A Yushkevich, Brian B Avants, John Pluta, Sandhitsu Das, David Minkoff, Dawn Mechanic-Hamilton, Simon Glynn, Stephen Pickup, Weixia Liu, James C Gee, Murray Grossman, and John A Detre. A high-resolution computational atlas of the human hippocampus from postmortem magnetic resonance imaging at 9.4 T. *NeuroImage*, 44(2):385–98, January 2009. ISSN 1095-9572. doi: 10.1016/j.neuroimage.2008.08.042. URL http://www.pubmedcentral.nih.gov/articlerender.fcgi?artid=2650508\&tool=pmcentrez\&rendertype=abstract.